Coexistence of surface oxygen vacancy and interface conducting states in $LaAlO_3/SrTiO_3$ revealed by low-angle resonant soft X-ray scattering

Ming Yang[1,] Ariando Ariando[2,3,*], Caozheng Diao[4], James C Lee[5,6], Kaushik Jayaraman[4], Mansoor B A Jalil[7], Serban Smadici[8], Shengwei Zeng[2], Jun Zhou[9], Weilong Kong[2], Mark B. H. Breese[4], Sankar Dhar[3], Yuan Ping Feng[2], Peter Abbamonte[5], Thirumalai Venkatesan[2], Andrivo Rusydi[2,4,*]*

[1] Department of Applied Physics, The Hong Kong Polytechnic University, Hung Hom, Hong Kong SAR, China

[2] Department of Physics, National University of Singapore, Singapore 117542, Singapore. E-mail: ariando@nus.edu.sg,

[3] NUSNNI-NanoCore, National University of Singapore, Singapore 117411, Singapore.

[4] Singapore Synchrotron Light Source, National University of Singapore, Singapore 117603, Singapore.

[5] Frederick Seitz Materials Research Laboratory, University of Illinois at Urbana-Champaign Urbana, Illinois 61801, USA.

[6] Brookhaven National Laboratory, Upton, New York 11973, USA.

[7] Department of Electrical and Computer Engineering, National University of Singapore 117576, Singapore.

[8] Dept. of Physics and Astronomy University of Louisville, KY 40292, USA.

[9] Institute of Materials Research and Engineering, Agency for Science, Technology and Research (A*STAR), 2 Fusionopolis Way Singapore 138634, Singapore

Keywords: perovskite oxide interface, surface oxygen vacancies, interface conducting states, low-angle resonant soft X-Ray scattering

Correspondence to who should be addressed: M.Y (mingyang@polyu.edu.hk), A. A. (phyarian@nus.edu.sg) or A. R. (andrivo.rusydi@nus.edu.sg)

Abstract

Oxide heterostructures have shown rich physics phenomena, particularly in the conjunction of exotic insulator-metal transition (IMT) at the interface between polar insulator $LaAlO_3$ and non-polar insulator $SrTiO_3$ ($LaAlO_3/SrTiO_3$). Polarization catastrophe model suggests an electronic reconstruction yielding to metallicity at both the interface and surface. Another scenario is the occurrence of surface oxygen vacancy at $LaAlO_3$ (surface-O_v), which predicts surface-to-interface charge transfer yielding metallic interface but insulating surface. To clarify the origin of IMT, one should probe surface-O_v and the associated electronic structures at both the surface and the buried interface simultaneously. Here, using low-angle resonant soft X-ray scattering (LA-RSXS) supported with first-principles calculations, we reveal the co-existence of the surface-O_v state and the interface conducting state *only* in conducting $LaAlO_3/SrTiO_3$ (001) films. *Interestingly*, both the surface-O_v state and the interface conducting state are absence for the insulating film. As a function of O_v density, while the surface-O_v state is responsible for the IMT, the spatial charge distribution is found responsible for a transition from two-dimensional-*like* to three-dimensional-*like* conducting accompanied by spectral weight transfer, revealing the importance of electronic correlation. Our results show the importance of surface-O_v in determining interface properties and provides a new strategy in utilizing LA-RSXS to directly probe the surface and buried interface electronic properties in complex oxide heterostructures.

1. Introduction

Since the discovery of an unexpected conducting interface in the atomically abrupt heterostructures comprised of $LaAlO_3$ and $SrTiO_3$ perovskite insulators,[1] many efforts have been devoted to unravelling the origin of this insulator-metal transition (IMT).[1–9] Along with the quasi two-dimensional (2D) conducting interface, various exotic properties that do not exist in their individual bulk counterparts have also been observed at the $LaAlO_3/SrTiO_3$ interface, such as Kondo scattering of metallic carriers, interfacial magnetism, and superconductivity.[5,10–19] It is believed that the key source of these fascinating properties is that $LaAlO_3$ is a highly polar insulator, which should result in a diverged polar potential with the increase of $LaAlO_3$ thickness. This leads to an important question – *how does the system overcome such a polar divergence*? The polar catastrophe model suggests that 0.5 electrons transferred from the $LaAlO_3$ surface into the interface can overcome the polar divergence, yielding both metallic interface and surface.[2–4] While this model can explain the observed conducting interface, it *cannot* explain the insulating $LaAlO_3$ surface and other phenomena.[7,9] Therefore, understanding of the surface and how it affects the interface are critical.

It is well-accepted that the emerging IMT property is dependent upon the growth condition. Transport measurements have shown that for samples grown at low oxygen partial pressure (P_{O2}) (~10^{-5} and 10^{-6} mbar), the interface is highly conducting with a carrier density of ~10^{17} cm^{-2}, and the conducting carriers extend deeply into the $SrTiO_3$ substrate.[5,6,14] For samples grown at higher P_{O2} (~ 10^{-3} and 10^{-4} mbar), on the other hand, the interface has a much lower carrier density of 1~2×10^{13} cm^{-2} with the carriers confined at the interface.[5,6,19] These observations were further confirmed by the atomic force microscopy measurement (AFM), as it revealed a broad carrier distribution for the samples prepared at low P_{O2} and a much narrower distribution for the samples prepared at high P_{O2}.[20] It has been reported that the varied P_{O2} could break the interface stoichiometry of $LaAlO_3/SrTiO_3$, which might affect interface

properties.[8,19] These results have indicated important roles of defects in the IMT and interfacial conductivity, and a previous study connected them to the effect of surface O_v.[21,22] First-principles calculations further highlighted that the occurrence of surface-O_v is the key for the 2D conducting interface and insulating surface,[7,9,19,23,24] which however, is yet to be directly confirmed with experimental evidence.

It is worth mentioning that transport measurements only probe partially of the total charge at the interface, lacking the information about the charge depth profile.[3,4] While other experimental techniques such as photoelectron spectroscopies[25,26] and transmission electron microscopy[22] had been applied but, as they are surface sensitive technique, they may alter the sample surface unintentionally, which in turn, influence its electronic structures. Therefore, an alternate, non-destructive experimental method is needed to unravel the surface-O_v and probe electronic structure from the surface to interface for these perovskite oxide heterostructures prepared under different growth conditions. Such measurement should reveal the underlying mechanism that results in IMT and enables us to understand the influence of preparation ambience on electronic properties of the system. In this study, by using low-angle resonant soft X-ray scattering (LA-RSXS) supported by first-principles calculations, we report a direct evidence of surface-O_v state in two-dimensional-*like* conducting $LaAlO_3/SrTiO_3$ interface. We further correlate the varied surface-O_v density with the different spatial distribution of interfacial charge changing from insulating, 2D-*like* and to three-dimensional (3D)-*like* conducting (together with O_v in the $SrTiO_3$) $LaAlO_3/SrTiO_3$ interface grown at various P_{O2}.

2. Results and discussion

Fabrication and characterization of $LaAlO_3/SrTiO_3$ heterostructures. As a model system, we design three $LaAlO_3/SrTiO_3$ heterostructures with different sheet resistances (R_s), at the P_{O2} of 1×10^{-1} mbar (sample S1, *insulating*), 1×10^{-3} mbar (sample S2, *2D-like* conductivity), and

1×10^{-6} mbar (sample S3, *3D-like* conductivity), respectively. The samples were grown by depositing a single crystal $LaAlO_3$ target on a TiO_2-terminated $SrTiO_3$ (001) substrate using pulsed laser deposition (see the details in Method). The thickness of $LaAlO_3$ films is chosen to be 26 unit cells (~9.9 nm) to ensure sufficient photon intensity for scattering and absorption and therefore we can probe the charge distribution from surface to interface. During the deposition, the growth mode was monitored using *in-situ* reflection high energy electron diffraction (RHEED). The observed RHEED oscillation (see **Figure 1a** indicates a layer-by-layer growth for all the samples grown at the different P_{O2}, in line with previous reports.[5,11] After deposition, all samples were cooled down to room temperature (RT) at the same P_{O2} during deposition. The surface morphology of the deposited films was studied using AFM. The samples S2 and S3 show similar surface roughness, as shown in **Figure 1b**, while the surface roughness of sample S1 slightly increases. The crystalline quality of all the three samples is revealed by the X-ray diffraction (XRD) results in **Figure1c**, which suggests that the three samples have the same crystalline structure, as their main characteristic peaks are overlap. From the XRD results, the minor shift in the sub-peaks at 48.3° might be related to varied surface structures of these three heterostructures, which will be discussed in detail later.

Transport and LA-RSXS measurement on $LaAlO_3/SrTiO_3$ heterostructures. The R_s, carrier density n and Hall mobility μ of these three model samples were measured using a Van-der-Pauw geometry. The temperature-dependent R_s of the low pressure grown sample S3 in **Figure 1d** shows 1 mΩ/□ at 5 *K* and increased to about 2.1 Ω/□ at RT, with a nearly constant carrier density of ~5.0×10^{16} cm^{-2} (see **Figure 1e**). This agrees with a *3D*-like conductivity as suggested by previous studies.[5,6] When the sample grown at a higher P_{O2} (sample S2), the R_s is significantly increased (see the blue curve in **Figure 1d**). It is about 14 kΩ/□ at RT and decreases to around 1 kΩ/□ at 5 *K*. Correspondingly, the associated carrier density varies slightly between 2.5×10^{13} cm^{-2} and 2.9×10^{13} cm^{-2}, as shown in **Figure 1f**. This temperature-

dependent conductivity is quasi-*2D* and has been ascribed to the coexistence of conducting electrons and localized electrons at the interface.[5,12] When the growth pressure is further increased (sample S1), the R_s increases beyond the measurement limit, showing an insulating behaviour.

The transport data suggest a transition of the electronic phase from an insulating, 2D conducting to 3D conducting state in these three representative samples, which are controlled by the P_{O2} during the growth. To further probe the electronic structures from the surface to the interface of these oxide heterostructures, we carried out non-destructive, element specific LA-RSXS measurements at O *K* (O 1*s* → 2*p*) and Ti $L_{3,2}$ (Ti $2p_{3/2,1/2}$ → 3*d*) edges. The LA-RSXS experiment is especially designed that the incoming photons were directed normal to the sample surface , while the angle of outgoing photon (θ_{out}) was varied from ~1.0° to ~20.0° with respect to the sample surface (see the illustration in **Figure 2**a). To validate our method, we first examine the LA-RSXS at Ti $L_{3,2}$ edges of the insulating sample S1. Due to the X-ray selection rule, Ti $L_{3,2}$ edges probe the transition from Ti 2*p* to Ti 3*d*, therefore these edges are sensitive to the presence of Ti ions. As **Figure 2b** shows, we only observe a flat background for the θ_{out} up to 5.0° (see also **Figure S1**, Supporting Information). This reveals that the signals are mainly from the $LaAlO_3$ layers. Interestingly, the features at Ti $L_{3,2}$ edges can be resolved (see **Figure 2b**) when the θ_{out} is further increased by only 0.5° (from 5.0° to 5.5°), which indicates a sharp electronic structure at the interface of the sample.

The photon penetration depth, L_p at very low angles (< ~10º) is governed by the following equation [27]:

$$L_p = \frac{\lambda}{4\pi} \frac{1}{Im\left(\sqrt{\theta^2 - 2\delta - 2iK}\right)} \quad (1)$$

where δ and K come from the definition of complex refractive index $N \equiv (1 - \delta) + i K$. For small angles, when θ increases, there is a rapid increase in the penetration depth. The photon penetration depth obtained from the X-ray tabulated value[28] for $LaAlO_3$ at 453.5 eV, which is just below the Ti L_3 main edge of STO, is presented in **Figure S3-1** (Supporting Information). It shows that the value at θ_{out} ~5º is ~ 10.6±1 nm whereas at ~5.5º, it is ~14.6±1 nm. Since the LAO film thickness is 10±1nm, therefore, when θ_{out} is ~5.5º, the photon starts probing Ti at the buried interface of LAO/STO and STO. This is consistent with LA-RSXS where Ti $L_{3,2}$ edges are now visible at θ_{out} ~ 5.5º as shown in **Figure 2**b.

Observation of surface oxygen vacancy and interface conducting states. Our main observations are the LA-RSXS results at O K edge for samples S1, S2, and S3 as shown in **Figure 3** and **Figure 2**c-d. **Figure S3-2** (Supporting Information) shows the LA-RSXS profiles of all three samples at different θ_{out}. The LA-RSXS is measured in total fluorescence yield (TFY) mode, which is a photon-in-photon-out measurement method which depends on θ_{out}. The data at 2.5º and 20º are shown in **Figure 3a-c**. The experimental data is scaled to the tabulated cross-section obtained from the X-ray tabulated value.[28] This gives us the extinction coefficient, K of the samples as shown in **Figure S3-2** (Supporting Information). From the penetration depth calculations, we find that when the $\theta_{out} < \sim 4.1°$, the resonant peaks are mainly from the O ions in the $LaAlO_3$ films (from the $LaAlO_3$ surface to the $LaAlO_3/SrTiO_3$ interface). Whereas, for θ_{out} above 4.1°, the peaks are contributed by the O from both the $LaAlO_3$ and $SrTiO_3$. For $\theta_{out} \sim 2.5°$, the photon penetration depth is estimated to be 3.7 ± 1.0 nm, therefore it reveals electronic structure near $LaAlO_3$ surface. For the insulating sample S1, we can see only a dominant peak at ~536.0 eV (**Figure 3a**), which is related to transitions from O 1s to hybridized O 2p / La 5d orbital at $LaAlO_3$ (see the PDOS in **Figure S4**, Supporting Information).[29] For a larger $\theta_{out} \sim 20.0°$, the photon penetration depth is estimated to be above

50 nm, thus it can detect the signals from both the $LaAlO_3$ films (~10 nm) and the $SrTiO_3$ substrate. A strong peak is observed at ~530.5 eV for the insulating sample S1, while the peak at 536.0 eV remains (the lower panel in **Figure 3a**). The peak at 530.5 eV is ascribed to transitions from O 1*s* to hybridized O 2*p* / Ti 3*d* orbitals in the $SrTiO_3$ near the interface (see the PDOS in **Figure S5**, Supporting Information).

Interestingly, at the small angle (θ_{out} ~ 2.5°) we find a new pre-peak for both 2D and 3D conducting samples. For the 2D conducting sample S2, the pre-peak is noticeable at ~530.5 eV. We would like to emphasize that the *effective* photon penetration depth at θ_{out} ~ 2.5° and ~530.5 eV is ~3.7 nm. Thus, this pre-peak is mainly coming from the $LaAlO_3$ surface. The intensity of this pre-peak grows rapidly as θ_{out} increases, and it is eventually resonant with the peak from $SrTiO_3$ as seen at higher θ_{out} (see the lower panels in **Figure 3b**). It is also found that the pre-peak is absent in the insulating sample and the occurrence of it in the conducting samples is accompanied by spectral weight transfer from higher energy structures, particularly 532.4 eV. Such a spectral weight transfer reveals the importance of electronic correlations resulting conducting interface and very different surface electronic structures between the insulating and conducting samples. Intriguingly, by comparing the conducting S2 and S3 samples (**Figure 3b-c**), the pre-peak in the 3D conducting sample is more pronounced than that of the 2D conducting sample. Based on the growth condition, sample S3 is expected to have a higher density of O_v, while samples S2 should have a lower density of O_v. Thus, the pre-peak in upper panels of **Figure 3b** and **3c** is a characteristic feature of O_v near the $LaAlO_3$ surface in the conducing $LaAlO_3/SrTiO_3$ samples. Further details of the pre-peak are given in **Figure S3-4** (Supporting Information).

Figure 2c shows the extinction coefficient *K* of the three samples as a function of θ_{out}. The figure shows the *K* taken at three different photon energies: an off-resonance of ~527 eV, pre-

peak of ~530.5 eV and the main O *K*-edge of ~536 eV. From the LA-RSXS in **Figure S3-2**, it is clear that the *K* is more or less the same for all sample for all θ_{out} when measured at ~527 eV (off-resonance) and ~536 eV (main O *K* edge). This is clearly seen in **Figure 2c** where *K* is similar for all three samples at these two energies. Interestingly, we see significant changes at the pre-peak ~530.5 eV, which is the centre of the discussion.

We next highlight that in LA-RSXS as a function of θ_{out} we are probing two different charges, i.e. (1) localized-*like* charges at and near the surface of LAO, which are due to the existence of the surface-*like* oxygen vacancies (surface-O_V), and (2) interface-*like conducting* charges at the $LaAlO_3/SrTiO_3$ interface, which are induced by a charge transfer due to the presence of O_V at the surface of $LaAlO_3$. We demonstrate the powerfulness of LA-RSXS to probe and distinguish these surface-*like* and interface-*like* charges in the complex oxide heterostructures. The LA-RSXS at a particular θ_{out} (shown in **Figure 2c**) means an accumulation of the *K* from each layer (or unit cell) till that particular angle and hence a particular depth. The *K* near the interface of $LaAlO_3$ and $SrTiO_3$ has a contribution from both the surface-O_V as well as the charge at the interface.

The *K* seen in **Figure 2c** at any particular angle, and hence a particular depth, is an accumulation of contribution from all the layers above that. To put it in simple terms, we can liken this to an integration of the layer-by-layer contribution till that depth. So, to get an idea regarding a layer-by-layer distribution, we take the first derivative of the quantity measured in **Figure 2c** to obtain **Figure 2d**, named ΔK_{charge}.

The dielectric susceptibility $\chi(\omega,\theta)$, is related to the extinction coefficient through the relation $\sqrt{1+\chi(\omega,\theta)} = (1-\delta(\omega,\theta)) + \mathrm{i}\,K(\omega,\theta)$. Scattering of X-rays from charges at a particular energy, gives us information about the charge distribution and about the dielectric susceptibility χ at that energy.[30] So, we argue that the variation of *K* is related to the spatial variation of dielectric susceptibility $\chi(z)$. In our case, the derivative ΔK_{charge} is qualitatively proportional to the charge density and gives us an idea about the nature of spatial variation of the same.

For further analysis, the ΔK_{charge} is fitted with a Lorentzian fitting resulting a full width at half maximum (FWHM) of ~ 1.8º for the S2M sample and FWHM of ~ 5.9º for the S3M sample. This reveals that the S2M sample has the charge distribution of 2D-*like* and is mostly concentrated and high in the $SrTiO_3$ near the $LaAlO_3/SrTiO_3$ interface, whereas in the case of the S3M sample, it is distributed 3D-*like* over $LaAlO_3$ to $SrTiO_3$ crossed the interface. Similar charge carrier distributions in the conducting $LaAlO_3/SrTiO_3$ heterostructures have been mapped previously using CT-AFM.[20] For further details, the penetration depth as a function of θ_{out} is plotted and discussed in **Figure S3-3** of Supporting Information.

First-principles calculations. To find the origin of those pre-peaks and its impact on the insulating surface and conducting interface, we perform first-principles calculations using four idealized models: (2×2×1) 5 layers of $LaAlO_3$ supercell on the $SrTiO_3$ (001) substrate without surface-O_v (as a representative of insulating), with one surface-O_v (see **Figure 4a**) (as representative of 2D-*like* conducting), with two surface-O_v (3D conducting) and with one surface-O_v and one interface-O_v (as representative of 3D-like conducting). From the layer-projected density of states (PDOS) for the $LaAlO_3/SrTiO_3$ interface without O_v (see **Figure S6**, Supporting Information), there are no mid-gap states observed. This corresponds with the LA-RSXS for the insulating sample S1 where no pre-peak is observed at small θ_{out}.

In contrast, the presence of O_v at the $LaAlO_3$ surface introduces a new mid-gap state (**Figures 4b** and **4c** and **Figures S7-S9** in Supporting Information). The PDOS also shows that such the surface of $LaAlO_3$ remains insulating due to a charge transfer from the surface to the interface. This mid-gap state is mainly ascribed to the *p* orbitals of the surface oxygen atoms, as well as weaker contribution from surface Al atoms. It is mainly from the surface layer as evidenced by the visualized partial charge density (blue colour in **Figure 4a**). The mid-gap state induced by the surface-O_v is resonant with the interfacial conducting states (**Figure 4c**) from the interfacial

Ti t_{2g} orbitals. This can be understood as the excess charges induced by surface-O_v are transferred into the interfacial TiO_2 layers to minimize the polar divergence in the $LaAlO_3$ layers.[7,9] Furthermore, in the case of $LaAlO_3/SrTiO_3$ heterostructure with higher density of O_v, for example, two surface-O_v in the model structure, it turns out that the mid-gap state becomes slightly more pronounced (**Figure 4d** and **Figures S11-S13** in Supporting Information).

It has been suggested that when the $LaAlO_3/SrTiO_3$ heterostructure is prepared at the lower P_{O2}, the O_v might occur in the $SrTiO_3$ substrate.[6,23] Indeed, from calculated layer dependent formation energy of O_v (see **Figure S11** in Supporting Information), we find that the formation of O_v at the $SrTiO_3$ interface is possible as its formation energy is the second lowest (the lowest one is for both O_v at the $LaAlO_3$ surface as we just discussed) for the oxygen deficient growth condition. This interfacial O_v introduces additional charge carriers, which extend much deeper into the $SrTiO_3$ substrate (see **Figure S14**, Supporting Information), thus lending to more pronounced 3D conductivity, compared with 2D conducting and insulating samples (see the comparison in **Figure S15**). These calculation results collaborate well with the experimental observations, which clearly suggest the existence of surface O_v in the conducting $LaAlO_3/SrTiO_3$ interface and unravel surface effects on the interface properties in the 2D-*like* conducting sample. While for the 3D-*like* conducting sample, the coexistence of the O_v near $LaAlO_3$ surface and the O_v in $SrTiO_3$ near the interface contributes to the more extended conducting carrier in the samples, in which the interfacial O_v introduces additional electronic states below Fermi level that can be decoupled with that of surface O_v (see **Figures S14**).

It is believed that the conducting interface of the $LaAlO_3/SrTiO_3$ heterostructure is due to the charge transfer from the $LaAlO_3$ layers into the Ti ions at the interface.[2,7,9,19] Our detailed LA-RSXS measurements and first-principles calculations show that surface-O_v is important for this charge transfer process and plays a critical role in the onset of interface conductivity. Without

surface-O_v, charge transfer is very weak, if any, thus resulting in an insulting behaviour as evidenced by the sample prepared at high P_{O2} (S1 sample). In this case, the O_v is either difficult to be formed or can be compensated by the high P_{O2}. In contrast, when the samples are prepared at a low P_{O2} (S2 sample), the formation of surface-O_v is favourable. Thus, the excess charges from the surface are transferred into the interfacial Ti ions, leading to the quasi-2D conducting interface while the surface remains insulating. When the samples are prepared at very low P_{O2} (S3 sample), more surface-O_v are formed, and the O_v might occur at the interface or even in the $SrTiO_3$ substrate.[6,31] These lead to a 3D-*like* conductivity and a very broad distribution of carrier density. From our theoretical calculations, the conducting $LaAlO_3/SrTiO_3$ (001) has two different electronic structures: (1) at the $LaAlO_3$ surface the insulating mid-gap state occurs due to surface-O_v and (2) at the $LaAlO_3/SrTiO_3$ interface the conducting interface state appears due to the charge transfer into Ti 3*d* orbital. The LA-RSXS reveals these two new states. When the detection angle θ_{out} is small, LA-RSXS directly probes the surface-O_v states at O *K* edge. When the θ_{out} is larger, the conducting interface state can be resolved at O *K* and Ti $L_{3,2}$ edges. Thus, by using LA-RSXS, we can probe spatial distribution electronic structure of $LaAlO_3$ surface down to the buried $SrTiO_3$ interface in the $LaAlO_3/SrTiO_3$. We note that in our LA-RSXS, the presence of surface-O_V state is not influenced by the intense synchrotron radiation beam evident by the absence of the pre-peak in the insulating sample S1. The sample was measured at room temperature.

3. Conclusion

In conclusion, we have shown a direct experimental evidence of co-existence of $LaAlO_3$ surface-O_v state and conducting interface charge state and the corresponding spatial charge distribution at the $LaAlO_3/SrTiO_3$ interface. Supported by first-principles calculations, the interfacial conductivity and the charge distribution are found to be strongly dependent on the surface-O_v accompanied by spectral weight transfer. Our result unravels the important role of

surface-O_v and electronic correlations in determining the electronic properties at the perovskite oxide interface and demonstrates a new capability of LA-RSXS in probing spatial distribution electronic structure from a surface to a buried interface of oxide heterostructures.

Materials and Methods

Sample Growth: To obtain a single TiO_2 terminated surface, $SrTiO_3$ were treated by buffered-HF and annealed at 950°C in oxygen environment.[32] With this treatment, an atomically flat $SrTiO_3$ surface is obtained and confirmed by clear unit cell height steps observed with atomic force microscopy.[5] Twenty-six unit cells of $LaAlO_3$ were deposited by using pulsed laser deposition and a single crystal $LaAlO_3$ target on the TiO_2-terminated (001) $SrTiO_3$ substrates in oxygen partial pressures ranging from 10^{-6} to 10^{-1} mbar at 850 °C. The films were grown using a laser energy with a fluency of 3 J/cm^2 and repetition rate of 1 Hz. The deposition was monitored by periodic RHEED oscillation, which clearly show the layer-by-layer growth for the $LaAlO_3$ films. After growth, all samples were cooled to room temperature at the same oxygen partial pressure used during the deposition.

Electrical Measurement: Van der Pauw geometry was employed to measure the sheet resistance, carrier density and Hall mobility of the three samples S1, S2 and S3. The wire connection for electrical transport measurement was done by Al ultrasonic wire bonding and the measurements were performed in Quantum Design Physical Property Measurement System (PPMS).

Low-angle Resonant Soft X-ray Scattering (LA-RSXS) Measurements: The LA-RSXS measurements were performed at the soft X-ray and ultraviolet (SUV) beamline of the Singapore Synchrotron Light Source and at the X1B beamline of National Synchrotron Light Source. [30,33] The LA-RSXS experiment was especially designed that the incoming photon was fixed parallel to the normal surface of the samples (with electric field of photon perpendicular

to the surface of the sample), while the angle of outgoing photon (θ_{out}) was varied from ~1° to ~20.0° with respect to the surface of the samples. The energy resolution was set to ≈0.25 eV. The results of LA-RSXS at the O *K* and Ti $L_{3,2}$ edges from the three samples with different outgoing angles are shown in Supporting Information 1 and 2. In order to extract the changes in electronic structure at the $LaAlO_3/SrTiO_3$ interface, we used $SrTiO_3$ bulk as reference. All the measurements were done at room temperature.

DFT Calculations: All the calculations were performed using density-functional-theory based Vienna ab initio simulation package (VASP5.4.18) with the Perdew–Burke–Ernzerhof (PBE) format exchange-correlation functional and the projector-augmented wave (PAW) pseudopotentials.[34–36] The cut-off energy for the expansion of plane-wave basis was set to 500 eV. The on-site Coulomb interaction has been considered with effective U=1.2 and U=11 adopted for ***d*** and ***f*** orbitals of Ti and La ions, respectively. The $LaAlO_3/SrTiO_3$ interfaces were modeled by placing five unit cells of (2×2×1) $LaAlO_3$ supercell on TiO_2-terminated $SrTiO_3$ (001) substrates with a thickness of 5 unit cells, in which we considered four interfaces structures: without O_v, with a surface-O_v, with two surface-O_v, and with one surface-O_v and one O_v at the interface TiO_2 sublayer. A vacuum with a thickness of 15 Å was applied normal to $LaAlO_3$ surfaces to minimize artificial Coulomb interaction between neighboring surfaces. 6×6×1 Gamma-point-centered k-point meshes were used for sampling Brillouin zones of the $LaAlO_3/SrTiO_3$ interface structures. The electronic convergence was set to 1.0×10^{-6} eV, and the force on each atom was relaxed to be smaller than 0.01 eV/Å with fixed bottom layer of the $SrTiO_3$ substrate. The dipole correction was applied to minimize artificial dipole interactions.[37]

Supporting Information

Supporting Information is available from the Wiley Online Library or from the author.

Acknowledgements

We acknowledge technical support and discussion with Jason Lim and Xiao Renshaw Wang. This work was supported by the Singapore National Research Foundation under its Competitive Research Funding (No. NRF-CRP 8-2011-06 and No. R-398-000-087-281), MOE-AcRF Tier-2 (MOE2015-T2-1-099, MOE2015-T2-2-065, and MOE2015-T2-2-147), NUS YIA, MOE AcRF Tier 1 (R-144-000-368-112, R-144-000-346-112, and R-144-000-364-112), and NUS Core Support (C-380-003-003-001). M. Y. would like to acknowledge the funding support from Hong Kong Polytechnic University (Project No.: 1-BE47 and ZE2F). We acknowledge Centre for Advanced 2D Materials and Graphene Research at National University of Singapore, and National Supercomputing Centre of Singapore for providing computing resource.

Conflict of Interest

The authors declare no conflict of interest.

Author Contributions: A.R., C.D., J.C.L., S.S. performed low-angle resonant soft X-ray scattering. A.A., S.W.Z, and T.V. prepared samples and perform transport and X-ray diffraction and RHEED measurements. M.Y., J.Z., M.J., W.K., A.R., Y.P.F. performed theoretical calculations. M.Y., K.J. and A.R. analyzed data comprehensively and wrote paper with inputs from all co-authors. A.R. designed the LA-RSXS for detecting the electronic structure at surface and interface. A.R. and A.A. initiated and led the project.

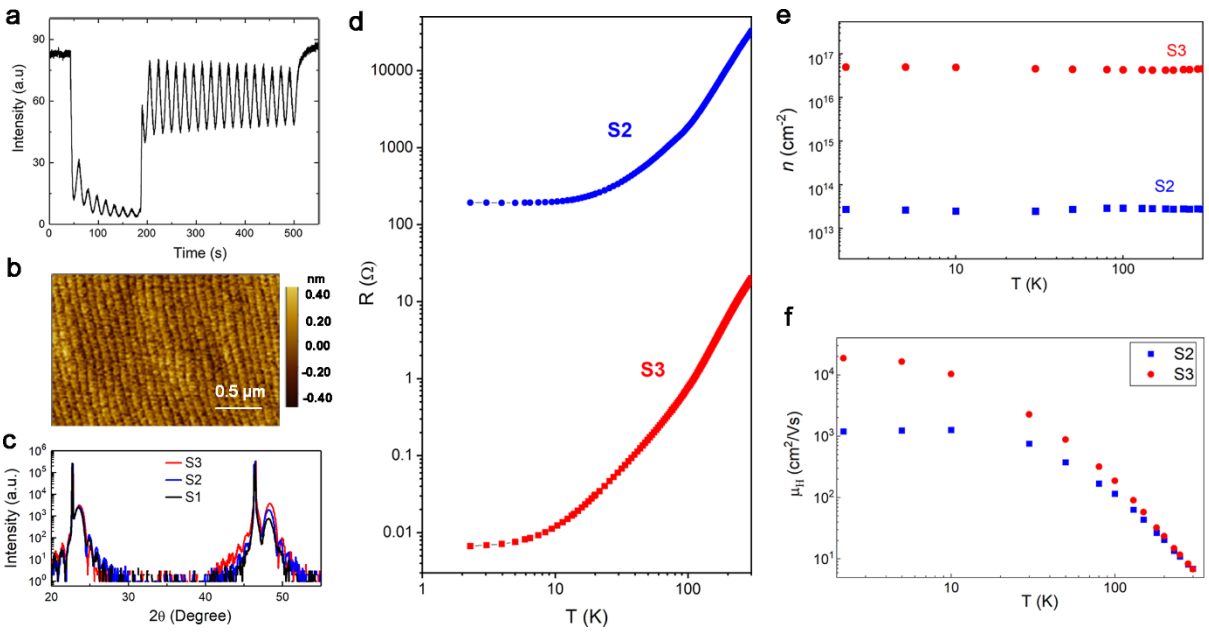

Figure 1. Structural and electric characterization of three $LaAlO_3/SrTiO_3$ (001) samples (S1-S3) grown at different oxygen partial pressures. (a) Reflection high-energy electron diffraction (RHEED) oscillations during deposition corresponding to 26 unit cells of $LaAlO_3$ on the $SrTiO_3$ (001) substrate terminated with TiO_2 layer. (b) The AFM image for sample S2. (c) X-ray diffraction (XRD) (log plot) for the samples S1-S3. (d-f) temperature dependent sheet resistance, carrier density and Hall mobility for sample S2 and S3.

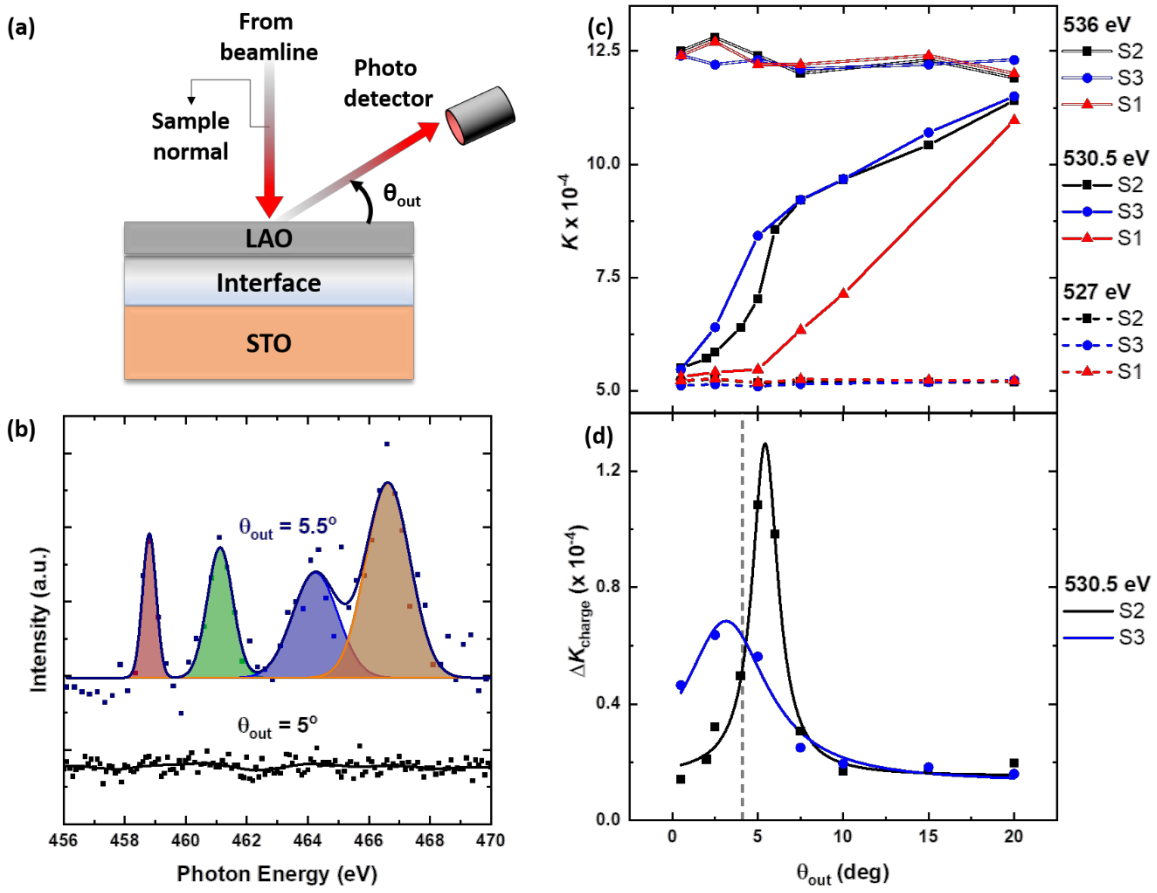

Figure 2. (a) Schematic diagram for the LA-RSXS measurements. (b) The LA-RSXS at Ti $L_{3,2}$ edges with the θ_{out} of 5.0° and 5.5° for sample S2. (c) The plot of extinction coefficient, K of all the samples at off-resonance (~527 eV), the pre-peak (~530.5 eV) and the main O 2p peak (~536 eV), respectively. (d) The first-derivative plot of K shown in (c), named ΔK_{charge}, at the pre-peak energy for the S2 (2D-*like*) and S3 (3D-*like*) samples, which represents the distribution of charge. The dashed line in **Figure 2d** around ~4.1° corresponds to a depth of ~10 nm, which is the thickness of the LAO layer.

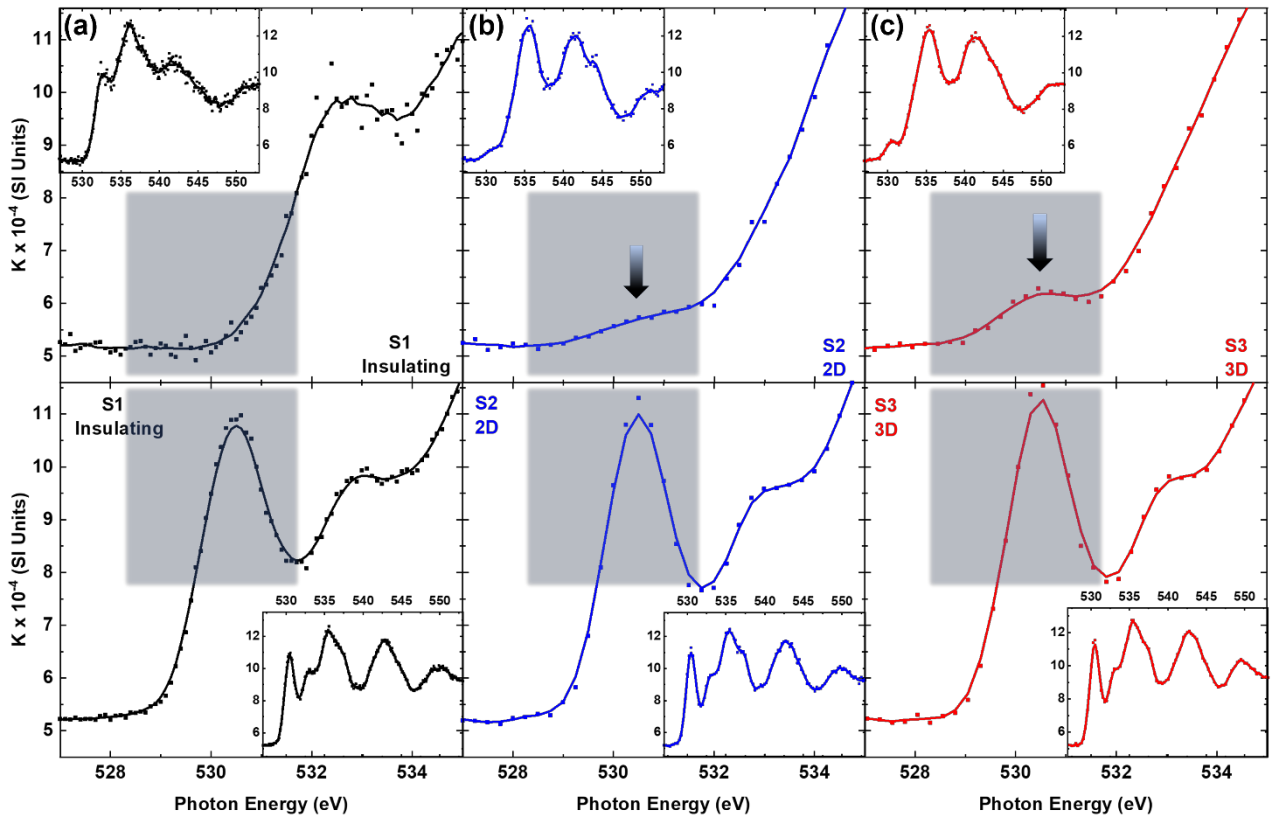

Figure 3. The LA-RSXSs at O *K* edge for sample (a) S1, (b) S2 and (c) S3 at the θ_{out} of 2.5º (top panel) and 20º (bottom panel). The new pre-peaks are highlighted. The insets show a wider energy range.

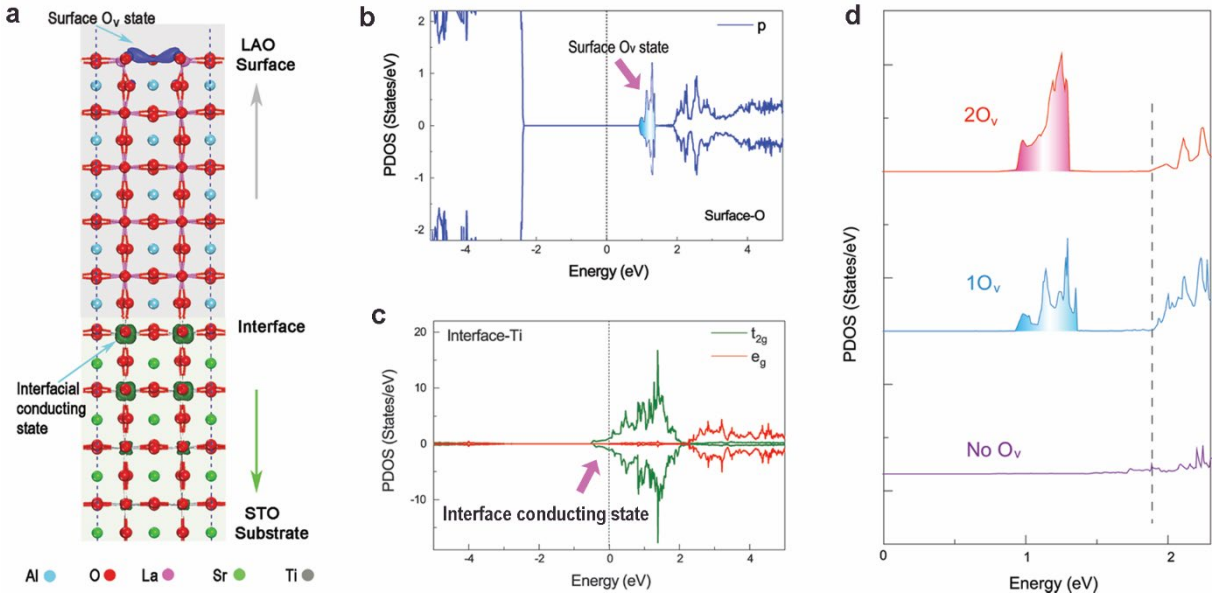

Figure 4. (a) An illustration of the atomistic structure of the $LaAlO_3/SrTiO_3$ heterostructure with a surface O_v, superimposed with the partial charge density of the surface O_v state (blue color) and interfacial Ti T_{2g} states (green color) using an iso-surface value of 1.0×10^{-3} e/Å^3. The PDOSs of (b) surface O and (c) interfacial Ti atoms, respectively, where the Fermi level is set to 0 eV. (d) The PDOSs (spin-up) of oxygen atoms at the surface AlO_2 layers for the $LaAlO_3/SrTiO_3$ heterostructures without the O_v, with one surface O_v, and with two surface O_v, where the vacuum level was used for the alignment.

Reference

[1] A. Ohtomo, H. Y. Hwang, *Nature* **2004**, *427*, 423.

[2] N. Nakagawa, H. Y. Hwang, D. A. Muller, *Nat. Mater.* **2006**, *5*, 204.

[3] S. Thiel, *Science* **2006**, *313*, 1942.

[4] T. C. Asmara, A. Annadi, I. Santoso, P. K. Gogoi, A. Kotlov, H. M. Omer, M. Motapothula, M. B. H. Breese, M. Rübhausen, T. Venkatesan, Ariando, A. Rusydi, *Nat. Commun.* **2014**, *5*, 3663.

[5] Ariando, X. Wang, G. Baskaran, Z. Q. Liu, J. Huijben, J. B. Yi, A. Annadi, A. R. Barman, A. Rusydi, S. Dhar, Y. P. Feng, J. Ding, H. Hilgenkamp, T. Venkatesan, *Nat. Commun.* **2011**, *2*, 188.

[6] Z. Q. Liu, C. J. Li, W. M. Lü, X. H. Huang, Z. Huang, S. W. Zeng, X. P. Qiu, L. S. Huang, A. Annadi, J. S. Chen, J. M. D. Coey, T. Venkatesan, Ariando, *Phys. Rev. X* **2013**, *3*, 021010.

[7] L. Yu, A. Zunger, *Nat. Commun.* **2014**, *5*, 5118.

[8] M. P. Warusawithana, C. Richter, J. A. Mundy, P. Roy, J. Ludwig, S. Paetel, T. Heeg, A. A. Pawlicki, L. F. Kourkoutis, M. Zheng, M. Lee, B. Mulcahy, W. Zander, Y. Zhu, J. Schubert, J. N. Eckstein, D. A. Muller, C. S. Hellberg, J. Mannhart, D. G. Schlom, *Nat. Commun.* **2014**, *5*, 5118 **2013**, *4*, 2351.

[9] J. Zhou, T. C. Asmara, M. Yang, G. A. Sawatzky, Y. P. Feng, A. Rusydi, *Phys. Rev. B* **2015**, *92*, 125423.

[10] N. Reyren, S. Thiel, A. D. Caviglia, L. F. Kourkoutis, G. Hammerl, C. Richter, C. W. Schneider, T. Kopp, A.-S. Ruetschi, D. Jaccard, M. Gabay, D. A. Muller, J.-M. Triscone, J. Mannhart, *Science* **2007**, *317*, 1196.

[11] A. Brinkman, M. Huijben, M. van Zalk, J. Huijben, U. Zeitler, J. C. Maan, W. G. van der Wiel, G. Rijnders, D. H. A. Blank, H. Hilgenkamp, *Nat. Mater.* **2007**, *6*, 493.

[12] J. A. Bert, B. Kalisky, C. Bell, M. Kim, Y. Hikita, H. Y. Hwang, K. A. Moler, *Nat. Phys.*. **2011**, *7*, 767.

[13] L. Li, C. Richter, J. Mannhart, R. C. Ashoori, *Nat. Phys.* **2011**, *7*, 762.

[14] J.-S. Lee, Y. W. Xie, H. K. Sato, C. Bell, Y. Hikita, H. Y. Hwang, C.-C. Kao, *Nat. Mater.* **2013**, *12*, 703.

[15] M. Salluzzo, S. Gariglio, D. Stornaiuolo, V. Sessi, S. Rusponi, C. Piamonteze, G. M. De Luca, M. Minola, D. Marré, A. Gadaleta, H. Brune, F. Nolting, N. B. Brookes, G. Ghiringhelli, *Phys. Rev. Lett.* **2013**, *111*, 087204.

[16] F. Bi, M. Huang, S. Ryu, H. Lee, C.-W. Bark, C.-B. Eom, P. Irvin, J. Levy, *Nat. Commun.* **2014**, *5*, 5019.

[17] R. Ohshima, Y. Ando, K. Matsuzaki, T. Susaki, M. Weiler, S. Klingler, H. Huebl, E. Shikoh, T. Shinjo, S. T. B. Goennenwein, M. Shiraishi, *Nat. Mater.* **2017**, *16*, 609.

[18] I. Božović, J. Levy, *Nat. Phys.* **2020**, *16*, 712.

[19] M. Yang, Ariando, J. Zhou, T. C. Asmara, P. Krüger, X. J. Yu, X. Wang, C. Sanchez-Hanke, Y. P. Feng, T. Venkatesan, A. Rusydi, *ACS Appl. Mater. Interfaces* **2018**, *10*, 9774.

[20] M. Basletic, J.-L. Maurice, C. Carrétéro, G. Herranz, O. Copie, M. Bibes, É. Jacquet, K. Bouzehouane, S. Fusil, A. Barthélémy, *Nat. Mater.* **2008**, *7*, 621.

[21] C. Cen, S. Thiel, G. Hammerl, C. W. Schneider, K. E. Andersen, C. S. Hellberg, J. Mannhart, J. Levy, *Nat. Mater.* **2008**, *7*, 298.

[22] K. Song, T. Min, J. Seo, S. Ryu, H. Lee, Z. Wang, S. Choi, J. Lee, C. Eom, S. H. Oh, *Adv. Sci.* **2021**, 2002073.

[23] N. Pavlenko, T. Kopp, E. Y. Tsymbal, G. A. Sawatzky, J. Mannhart, *Phys. Rev. B* **2012**, *85*, 020407.

[24] L. Zhang, X.-F. Zhou, H.-T. Wang, J.-J. Xu, J. Li, E. G. Wang, S.-H. Wei, *Phys. Rev. B* **2010**, *82*, 125412.

[25] M. Sing, G. Berner, K. Goß, A. Müller, A. Ruff, A. Wetscherek, S. Thiel, J. Mannhart, S. A. Pauli, C. W. Schneider, P. R. Willmott, M. Gorgoi, F. Schäfers, R. Claessen, *Phys. Rev. Lett.* **2009**, *102*, 176805.

[26] C. Cancellieri, M. L. Reinle-Schmitt, M. Kobayashi, V. N. Strocov, T. Schmitt, P. R. Willmott, S. Gariglio, J. M. Triscone, *Phys. Rev. Lett.* **2013**, *110*, 137601.

[27] L. G. Parratt, *Phys. Rev.* **1954**, *95*, 359.

[28] B. L. Henke, E. M. Gullikson, J. C. Davis, *At. Data Nucl. Data Tables* **1993**, *54*, 181.

[29] N. Palina, A. Annadi, T. C. Asmara, C. Diao, X. Yu, M. B. H. Breese, T. Venkatesan, A. Ariando, A. Rusydi, *Phys. Chem. Chem. Phys.* **2016**, *18*, 13844.

[30] P. Abbamonte, L. Venema, A. Rusydi, G. A. Sawatzky, G. Logvenov, I. Bozovic, *Science* **2002**, *297*, 581.

[31] A. Chikina, F. Lechermann, M.-A. Husanu, M. Caputo, C. Cancellieri, X. Wang, T. Schmitt, M. Radovic, V. N. Strocov, *ACS Nano* **2018**, *12*, 7935.

[32] M. Kawasaki, K. Takahashi, T. Maeda, R. Tsuchiya, M. Shinohara, O. Ishiyama, T. Yonezawa, M. Yoshimoto, H. Koinuma, *Science* **1994**, *266*, 1540.

[33] X. J. Yu, C. Z. Diao, T. Venkatesan, M. B. H. Breese, A. Rusydi, *Rev. Sci. Instrum.* **2018**, *89*, 113113.

[34] G. Kresse, J. Hafner, *Phys. Rev. B* **1993**, *47*, 558.

[35] G. Kresse, J. Hafner, *Phys. Rev. B* **1993**, *48*, 13115.

[36] P. E. Blöchl, *Phys. Rev. B* **1994**, *50*, 17953.

[37] L. Bengtsson, *Phys. Rev. B* **1999**, *59*, 12301.